

# Active BiVO<sub>4</sub> Swimmers Propelled by Depletion Gradients Caused by Photodeposition

Martin Wittmann, Maximilian Voigtmann, and Juliane Simmchen\*

Artificial active matter often self-propels by creating gradients of one or more species or quantities. For chemical swimmers, most frequently either O<sub>2</sub> or H<sup>+</sup> that are created in certain catalytic reactions are causing the interfacial flows which drive the self-propulsion. While the palette of reactions is extending constantly, especially toward more bio-compatible fuels, the depletion of species is often overlooked. Here, the photodeposition of metal species on BiVO<sub>4</sub> micro swimmers is considered. During the photodeposition reaction, metal ions are removed from the solution creating a depleted region around the particle. The ability of this depletion to drive active motion of artificial micro swimmers, as well as the influences of different metal ions and counter ions on the motion are investigated and cross compared.

## 1. Introduction


Self-phoretic propulsion was first described by Anderson,<sup>[1]</sup> and later Golestanian and Liverpool defined it as “gradients of (at least) a quantity” created through the swimmer itself.<sup>[2]</sup> This gradient sets interfacial processes in progress, and establishes a gradient of chemical potential along the surface of the swimmer, resulting in an imbalanced osmotic effect within the interfacial layer, which drives phoretic flows and ultimately causes the propulsion of the colloid. Looking at the most frequent propulsion reaction



it is undisputed that several different species can be the predominant cause of motility. The peroxide degradation happens

M. Wittmann, M. Voigtmann, J. Simmchen  
Chair of Physical Chemistry  
TU Dresden  
01069 Dresden, Germany  
E-mail: julianesimmchen@gmx.net

J. Simmchen  
Pure and applied Chemistry  
University of Strathclyde  
Glasgow G1 1BX, UK

 The ORCID identification number(s) for the author(s) of this article can be found under <https://doi.org/10.1002/smll.202206885>.

© 2023 The Authors. Small published by Wiley-VCH GmbH. This is an open access article under the terms of the Creative Commons Attribution License, which permits use, distribution and reproduction in any medium, provided the original work is properly cited.

DOI: 10.1002/smll.202206885

with many intermediate steps,<sup>[3]</sup> so that not only the molecular O<sub>2</sub> but also positively charged H<sup>+</sup> ions and even the peroxide itself are frequently considered.<sup>[2,4]</sup> Effects of diffusion have been incorporated frequently, considering peroxide-driven swimmers,<sup>[5]</sup> but also in other systems<sup>[6]</sup> where the diffusivities are of pivotal importance. The pool of chemical reactions able to propel active matter strongly diversified in the last years, showing that catalytic reactions beyond H<sub>2</sub>O<sub>2</sub> and hydrazine degradation can yield motility. We showed that redox reactions such as galvanic replacements, leading to overlaying gradients of metal and counter ions lead to rather efficient

propulsion,<sup>[6]</sup> even without bubble formation.<sup>[7–9]</sup> The consideration of ionic species has attracted some attention<sup>[10,11]</sup> even under the influence of light.<sup>[12,13]</sup> Theoretical considerations revealed that the assumption of thin Debye layers caused by dilute electrolytes might be an oversimplification.<sup>[14]</sup> DeCorato et al. have shown theoretically that the release of ions and the subsequent ionic strength resulting in the solutions can lead to qualitatively different behaviors when compared to standard phoretic mechanisms.<sup>[14]</sup> For most reported chemical micromotors, these phoretic mechanisms were based on the release of molecules or ions during the reaction, leading therefore to an increased number of species, creating a gradient. Here, we consider an example where the photo-induced depletion of a species is driving the particle motility. To do so, we chose a BiVO<sub>4</sub> mediated reductive photodeposition of different metal salts and complexes and observe the velocity and geometric position the particles assume during active motion (Figure 1).

## 2. Results and Discussion

BiVO<sub>4</sub> is a well-known photocatalyst with a bandgap ≈2.4eV,<sup>[15]</sup> which offers the additional advantage over other materials of clearly separated charge carrier accumulation on {010} and {110} facets. We could prove that this leads to efficient propulsion without the physical deposition of a Janus material.<sup>[16]</sup> This is true for different fuels from the well-known H<sub>2</sub>O<sub>2</sub>,<sup>[17]</sup> to organic amine oxidations.<sup>[18]</sup> Another recognized feature is the photodeposition of co-catalysts on these specific facets,<sup>[19]</sup> which cannot only favorably affect the photocatalytic properties and the charge carrier availability but also enhance the intrinsic asymmetry. Hypothesizing that the photodeposition

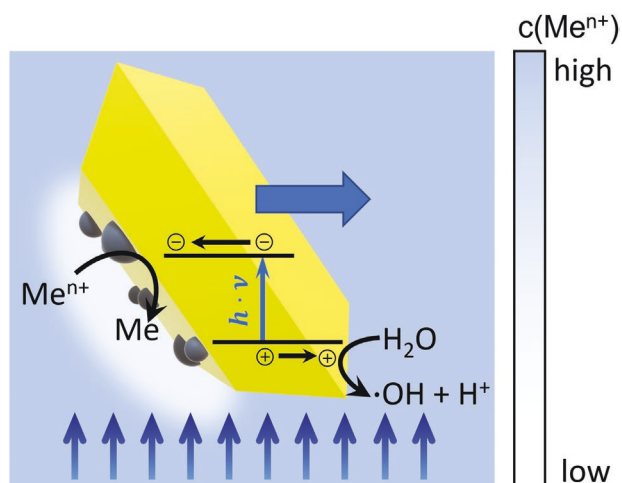


**Figure 1.** Schematic illustration of motion of a  $\text{BiVO}_4$  micro crystal driven by depletion of metal ions by a photodeposition reaction. Absorption of blue light creates electron hole pairs, where the excited electrons carry out the reduction of a metal ion on the  $\{010\}$  facets, while oxidation reactions are catalyzed by the holes on the  $\{110\}$  facets.

on the  $\{010\}$  facet would create a localized negative concentration gradient, able to propel active motion, we dispersed  $\text{BiVO}_4$  micro crystals in a solution of  $\text{AgNO}_3$  and irradiate with blue light ( $469 \text{ nm}$ ,  $4 \text{ W cm}^{-2}$ ). Initially, when only weak illumination for visualization purposes is present, the square shaped crystals lie flat and show Brownian motion, see Supporting Information. Upon irradiation, we observe a reorientation, leading to a stand-up behavior similar to the one we and others observed for  $\text{BiVO}_4$  polycrystals,<sup>[16,20]</sup> followed by active motion. Notably, this effect is already observed at concentrations as low as  $10^{-7} \text{ M}$ . The velocity increases with growing concentration of  $\text{AgNO}_3$ , but decreases, when the electrical conductivity caused by  $\text{AgNO}_3$  becomes dominant over the conductivity caused by dissolved  $\text{CO}_2$  (red squared in **Figure 2A**). A similar trend can be followed when looking at the mean squared displacement (MSD), which can be found in the Supporting Information.

While the earlier reported polycrystals showed either upright swimming or flat gliding, here, the reorientation seems to

happen continuously. The resulting swimming angle can be measured by the changes in dimensions of the particle in the microscopy image, as illustrated in **Figure 2B**. Here, we quantified this behavior by introducing an angle  $\alpha$ , that was determined from videomicroscopy as described in the Supporting Information. Swimming orientations of active Janus particles are known to be the result of chemical gradients, hydrodynamic flows, gravity, and second order influences.<sup>[21]</sup> However, the swimming vector parallel to the substrate was found to be not limited, neither to catalytic micromotors<sup>[6]</sup> nor to spherical particle geometries.<sup>[16,22]</sup> Experimentally, we found that the swimming orientation is also influenced by the environment, such as the pH value.<sup>[16,22]</sup> A very dominant influence is to be ascribed also to the ionic strength found in the solution, which directly affects the repulsion between substrate and particle and thereby the swimming height and the drag the particle is experiencing.

More in-depth modeling of specific influences on the orientation is limited by the available analytical data and the correlation to modeling factors. To overcome this, we measured the swimming angles depending on the  $\text{AgNO}_3$  concentration and correlated them with speed data and the conductivities in the solution. Overall, the swimming angle  $\alpha$  follows a similar trend as the velocity (**Figure 2C**). At the lowest concentration of  $10^{-7} \text{ M}$   $\text{AgNO}_3$  it is only  $\approx 10^\circ$ , and increases up to  $50^\circ$  at  $10^{-5} \text{ M}$ . This observation correlates well with the swimming speeds. However, since we cannot independently vary the speed from conductivity or swimming angle, it is experimentally impossible to distinguish whether the speed is dependent on, or resulting from the swimming angle.

Propulsion is accomplished by spatially separated reduction and oxidation reactions taking place on different facets of the micro crystals. The occurrence of photodeposition of the metal as reduction reaction was confirmed by several methods, including scanning electron microscope (SEM) and energy dispersive spectroscopy (EDX) analysis of the final products (**Figure 3A** and Supporting Information). The SEM image also demonstrates the selective occurrence of the reduction reaction only on the  $\{010\}$  facets of the micro crystals. For  $\text{AgNO}_3$ , the decrease in Ag concentration was also followed via inductively coupled plasma in connection with an optical emission spectrometer (ICP-OED) (Supporting Information). The oxidative

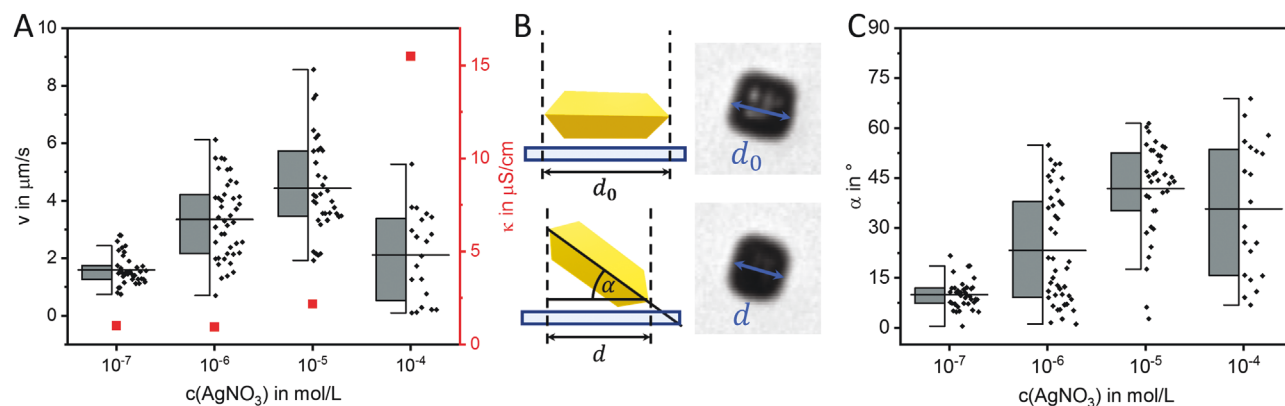


**Figure 2.** Motion in  $\text{AgNO}_3$ : A) box plot of velocities of  $\text{BiVO}_4$  micro crystals in different concentrations of  $\text{AgNO}_3$  under irradiation with blue light ( $469 \text{ nm}$ ,  $4 \text{ W cm}^{-2}$ ), electrical conductivities of solutions shown in red, B) schematic illustration of stand up behavior during motion and determination of the swimming angle  $\alpha$ , C) box plot of  $\alpha$  of  $\text{BiVO}_4$  micro crystals in different concentrations of  $\text{AgNO}_3$ .

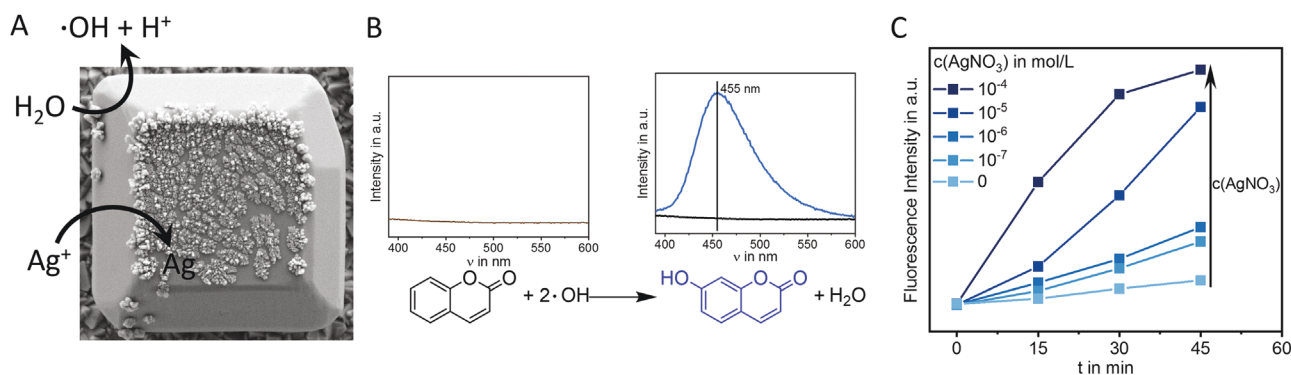


**Figure 3.** A) SEM image of a BiVO<sub>4</sub> micro crystal after photodeposition in  $5 \times 10^{-5}$  M AgNO<sub>3</sub>, B) scheme showing reaction of coumarin with OH<sup>•</sup> to fluorescent 7-hydroxycoumarin, C) fluorescent intensity of BiVO<sub>4</sub> solutions containing  $10^{-4}$  M coumarin and different concentrations of AgNO<sub>3</sub> after 15, 30 min and 45 min of irradiation with blue light.

side of this process is less obvious and most likely several reactions are involved. One possible oxidation reaction is the oxygen evolution reaction: While the band position of BiVO<sub>4</sub> is suitable for water oxidation, both, a high recombination rate as well as a short diffusion length, are inhibiting this reaction. Another likely option is the formation of OH<sup>•</sup> radicals. To verify this theory, OH<sup>•</sup> radicals are detected using coumarin as probe molecule, that reacts to 7-hydroxycoumarin upon contact with OH<sup>•</sup> (Figure 3B).<sup>[23]</sup> The formed 7-hydroxycoumarin can later be detected by its strong fluorescent emission at 455 nm (Supporting Information). Experiments in a bulk setup with different concentrations of AgNO<sub>3</sub> found the formation of increasing amounts of OH<sup>•</sup> radicals with increasing concentration of AgNO<sub>3</sub> and irradiation time (Figure 3B), proving that the OH<sup>•</sup> radical formation, accompanied by proton generation is clearly playing a role and neutralizes the overall reaction. Additionally, BiVO<sub>4</sub> is known to undergo photocorrosion, which is accompanied by a release of vanadates from the crystal lattice into the solution.<sup>[24]</sup> After performing photodeposition reactions with Pt, especially when caused by UV light, we detected the presence of vanadates in the supernatant via ICP-OES (data not shown). The concentration is very small but cannot be neglected completely as involved in the oxidative part of the equation.

Summarizing, the main reactions occurring on the surface of BiVO<sub>4</sub> are the reduction of Ag<sup>+</sup> to Ag on the {010} facets and the oxidation of H<sub>2</sub>O to OH<sup>•</sup> and H<sup>+</sup> on the {110} facets. As the reductive side consumes Ag<sup>+</sup>, a negative gradient in Ag<sup>+</sup> concentration is created. The resulting depleted region is characterized by an excess of counter ions (here NO<sub>3</sub><sup>-</sup>). Therefore, concentrations of at least four species have to be considered: OH<sup>•</sup>, H<sup>+</sup>, Ag<sup>+</sup> and NO<sub>3</sub><sup>-</sup>. Since the NO<sub>3</sub><sup>-</sup> counter ions are not involved in the overall reaction, there is no gradient formation to be observed and their contribution limits to the possible establishment of an additional electric field. Also, we expect OH<sup>•</sup> radicals to be of less impact, as they are highly reactive and very short lived and recombine readily with their surroundings. Therefore, we conjecture that the dominating influence is caused by the Ag<sup>+</sup> depletion gradient, which is much more persistent compared to the oxidative H<sup>+</sup> gradient (compare the diffusion coefficients of  $D(H^+) = 9.31 \times 10^5 \text{ cm}^2 \text{ s}^{-1}$  and  $D(\text{Ag}^+) = 1.65 \times 10^{-5} \text{ cm}^2 \text{ s}^{-1}$ ).

Considering that the photodeposition of metals on BiVO<sub>4</sub> is a rather unspecific reaction, a large variety of metals can

be used and we expand our considerations to copper. Overall, the speed of motion in copper solutions is lower, than the one we observed in AgNO<sub>3</sub>. This is in line with our expectations, because of their respective positions in the galvanic series. While silver has a standard potential of 0.8eV, the transition



is characterized by a normal potential of 0.34 eV. To allow photodeposition, the reduction/oxidation potential of the metal (oxides) to be deposited must be at favorable positions with regard to the energy-band positions of the semiconductor; that is, the conduction band (E vs NHE scale) must be more negative than the reduction potential of metals. Even though this is the case for the reduction of Cu<sup>2+</sup> (Figure 4A) the driving force is weaker than for Ag<sup>+</sup>, possibly causing a lower reaction rate and smaller gradients. In order to analyse the impact of the counter ion, experiments were carried out in the Cu<sup>2+</sup> salts CuCl<sub>2</sub>, CuSO<sub>4</sub>. The counter ions Cl<sup>-</sup> and SO<sub>4</sub><sup>2-</sup> possess different charges and diffusion coefficients ( $D(\text{Cl}^-) = 2.03 \times 10^{-5} \text{ cm}^2 \text{ s}^{-1}$  and  $D(\text{SO}_4^{2-}) = 0.96 \times 10^{-5} \text{ cm}^2 \text{ s}^{-1}$ ) (see Figure 4B). However, no significant differences were observed in the swimming behavior (Figure 4A), implying that the diffusion of these different ions happens mainly in the bulk and therefore does not have a major influence on the interfacial layer, where the flows that drive the active motility of the particles arise from the deposition of metal, here copper (Figure 4C), and the respective depletion gradient.

To further evaluate the influence of the deposited metal, we expand the materials to the noble metals gold and platinum. Due to solubility issues, both metals are not available as pure salts but rather in their complex form as tetrachloro- and hexachloro- complexes (HAuCl<sub>4</sub> and H<sub>2</sub>PtCl<sub>6</sub>), respectively. Looking at the standard potentials, we would expect the driving force for the reduction reaction to be rather high. By SEM and EDX analysis we again observe the deposition of the respective metal (Figure 5A,C). However, looking at the experimentally obtained swimming speeds in 10<sup>-5</sup> M solutions, both show lower motilities compared to their non-complexed cousin AgNO<sub>3</sub> (Figure 5B). We conjecture that the difference in velocity is heavily influenced by the reaction rate: while Ag<sup>+</sup> ions can freely react, the central atoms of the complexes have to leave their stable complex

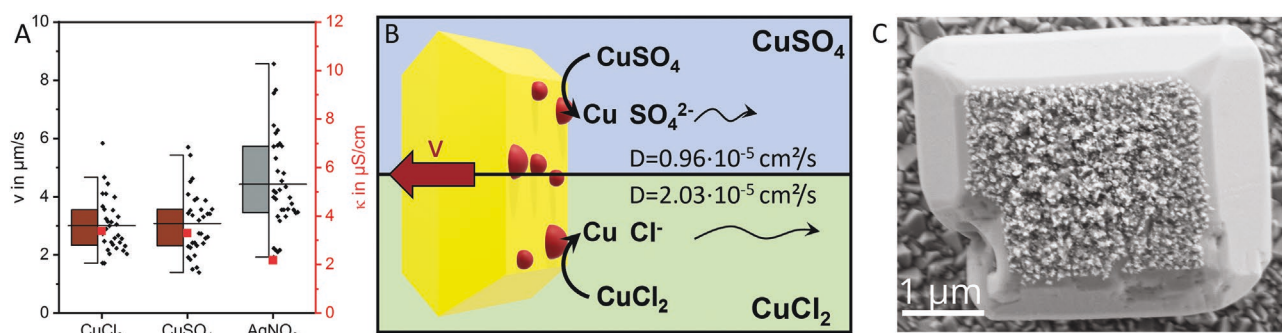


**Figure 4.** Influence of counter ion: A) box plot of velocities of  $\text{BiVO}_4$  micro crystals in  $\text{CuCl}_2$ ,  $\text{CuSO}_4$  and  $\text{AgNO}_3$  (all concentrations are  $10^{-5} \text{ M}$ ) under irradiation with blue light ( $469 \text{ nm}$ ,  $4 \text{ W cm}^{-2}$ ), electrical conductivities of solutions shown in red, B) schematic illustration of the differences in diffusion coefficient of the counter ions  $\text{Cl}^-$  and  $\text{SO}_4^{2-}$ , C) SEM images of  $\text{BiVO}_4$  micro crystals after photodeposition in  $5 \times 10^{-5} \text{ M}$   $\text{CuCl}_2$  on FTO.

environment in order to react with the photogenerated electrons. Yet another factor that has been discussed in relation to the efficiency of photodeposition<sup>[25]</sup> is the adsorption coefficient of the species that need to be reduced on the colloids. With a point of zero charge of  $\text{pH } 2.7$ <sup>[26]</sup>  $\text{BiVO}_4$  crystals are negatively charged at  $\text{pH} > 2.7$ , so the adsorption of positive  $\text{Ag}^+$  is expected to be favored over the adsorption of negatively charged complexes. In addition, both complex salt solutions exhibit a higher electrical conductivity (due to the high motility of the  $\text{H}^+$  ions), which also is known to quench the motion of micro swimmers.

Interestingly, trials to use oxidative photodeposition for the creation of motion did not succeed. While non-noble oxides such as  $\text{Co}_3\text{O}_4$  or  $\text{MnO}_2$  deposit readily at the  $\{110\}$  facets, these deposition processes do not cause active motility. Whether this effect is due to geometrical constraints, the involved electromotive forces or the ion balances, is yet unknown.

### 3. Conclusion

In summary, we demonstrated that  $\text{BiVO}_4$  micro crystals with intrinsic asymmetry can be propelled by photodeposition of

metal ions. The motion is accompanied by a reorientation with a swimming angle  $\alpha$  that can be measured from the microscopy images. The photoreduction reaction consumes metal ions and creates a negative concentration gradient. Propulsion was observed at concentrations below the  $\mu\text{M}$  range, which points toward a rather efficient reaction. The selective occurrence of the photoreduction reaction, selectively taking place on the  $\{010\}$  facets of  $\text{BiVO}_4$ , was confirmed by SEM analysis. To confirm the counter reaction, the formation of  $\text{OH}^\bullet$  radicals on the oxidative side of the process was verified using coumarin as a probe molecule. With a highly versatile reaction such as photodeposition, we found that the standard potential of the reaction determines the overall swimming speed. When investigating the impact of the counter ion on the motion using different  $\text{Cu}^{2+}$  salts, no significant influence was observed. Quite in contrast, the choice of the metal ion and its chemical nature, strongly affected the motion of the particles, which could be related to the chemical identity of the ion. Overall the results indicate that not only the creation of molecules but also their depletion can lead to active motion on the microscale. While this result is of fundamental nature and interest, it could be used to remediate contaminations in the environmental context.

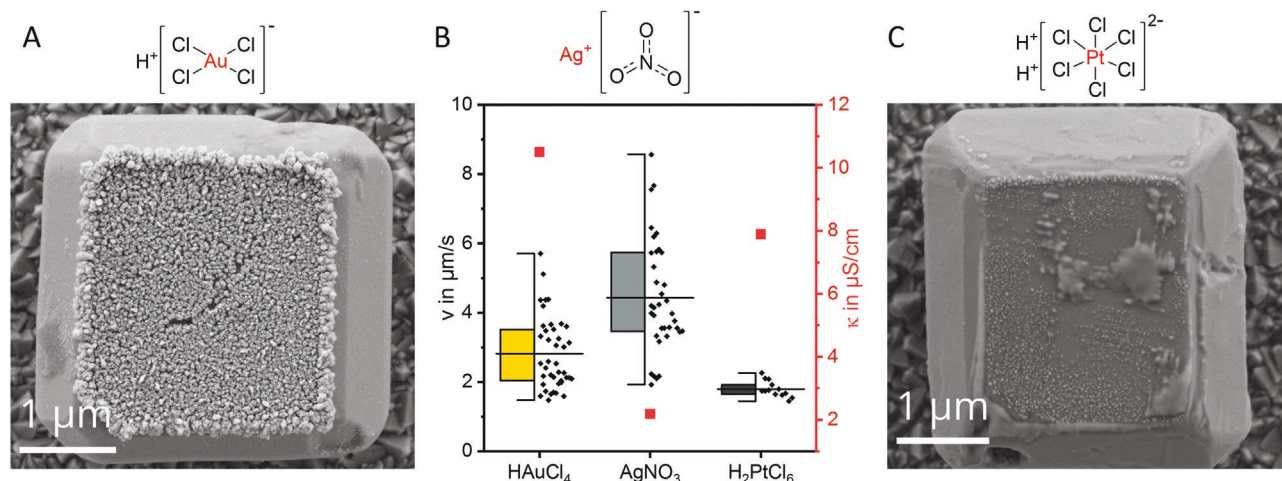


**Figure 5.** A) SEM image of a  $\text{BiVO}_4$  micro crystal after photodeposition in  $5 \times 10^{-5} \text{ M}$   $\text{HAuCl}_4$ , B) box plot of velocities of  $\text{BiVO}_4$  micro crystals in  $\text{HAuCl}_4$ ,  $\text{AgNO}_3$  and  $\text{H}_2\text{PtCl}_6$  (all concentrations are  $10^{-5} \text{ M}$ ) under irradiation with blue light ( $469 \text{ nm}$ ,  $4 \text{ W cm}^{-2}$ ), electrical conductivities of solutions shown in red, C) SEM image of a  $\text{BiVO}_4$  micro crystal after photodeposition in  $5 \times 10^{-3} \text{ M}$   $\text{H}_2\text{PtCl}_6$ .

## 4. Experimental Section

**BiVO<sub>4</sub> Particles:** BiVO<sub>4</sub> particles were synthesized by a hydrothermal reaction.<sup>[27]</sup> First, Bi(NO<sub>3</sub>)<sub>3</sub> · 5H<sub>2</sub>O (5 mmol, 2.4245 g) was dissolved in 20 mL 2 M HNO<sub>3</sub>, before NH<sub>4</sub>VO<sub>3</sub> (5 mmol, 0.5849 g) was added under stirring leading to a yellow solution. The pH was adjusted to pH 2 by slowly adding NH<sub>3</sub> (16% in H<sub>2</sub>O). NaCl was added to a concentration of 0.05 M and sodium dodecyl sulfate (SDS) to a concentration of 0.005 M. After 15 min of stirring, the solution was transferred to a teflon lined autoclave and aged for 2 h followed by a hydrothermal treatment at 200 °C for 24 h. Finally, the obtained solution was washed three times with MilliQ water.

**Microscopy Experiments:** Microscopy experiments were carried out using an inverted Zeiss microscope. 14 μm;L MilliQ water, 2 μm;L of metal salt solution, and 4 μm;L of a 2 mg mL<sup>-1</sup>

suspension of the BiVO<sub>4</sub> particles were placed on a plasma cleaned glass slide with an imaging spacer (diameter: 9 mm, height: 0.12 mm). Because the BiVO<sub>4</sub> particles have a significantly larger density than water, they quickly sink to the bottom of the glass slide, where their 2D trajectories parallel to the substrate can be recorded. The particles were irradiated with blue light (469 nm, 4 W cm<sup>-2</sup>) using a Colibri 7 light source. The videos were recorded with 40 frames per second for at least 1000 frames.

**Video evaluation:** The videos were analyzed using a code adapted by Zuyao Xiao using the MATLAB R2022a software. Therein, coordinates of the particles were obtained using the regionprops command on the binarized image and velocities were calculated as average instantaneous speeds between the frames. Exemplary trajectories are given in the Supporting Information. MSD analysis was carried out using the msdanalyzer Matlab class.<sup>[28]</sup>

**The Swimming Angle:** The swimming angle was determined by evaluating the visible area of the micro crystal using Matlab software. More details are given in the Supporting Information and the code is made available in zenodo (here doi.org/10.5281/zenodo.7486623).

**Detection of OH<sup>-</sup>:** Detection of OH<sup>-</sup> was done using coumarin as a probe molecule.<sup>[23]</sup> 2.2 mL of a solution containing 2.5 mg mL<sup>-1</sup> BiVO<sub>4</sub> particles, 10<sup>-4</sup> M coumarin and the noble metal salt was transferred to a quartz cuvette and irradiated using a Opsytec solo P Blue LED (450 nm) under stirring for 45 min. Aliquots of 0.2 mL were taken after 0, 15, 30, and 45 min, and particles were removed by centrifugation. The formed 7-hydroxycoumarin was detected by measuring the fluorescence intensity at 455 nm with excitation at 332 nm using a Horiba FluoroMax-4 Spectrofluorometer.

**SEM, Conductivity, and ICP Measurements:** SEM measurements were carried out with a ZEISS Ultra Gemini 2 using an SE2 detector.

Conductivity measurements were carried out using a Knick 703 Laboratory Conductivity Meter.

ICP measurements were carried out using a ICP-OES Perkin Elmer Optima 7000DV.

## Supporting Information

Supporting Information is available from the Wiley Online Library or from the author.

## Acknowledgements

The authors thank Dr. Sandra Heckel for fruitful discussions and help in the early stages of the project. All authors are grateful for generous funding from the Volkswagen foundation (grant nr. 91619), the Fulbright foundation for the Cottrell award and the DFG for the DFG-ANR project RODROLLS.

Open access funding enabled and organized by Projekt DEAL.

## Conflict of Interest

The authors declare no conflict of interest.

## Data Availability Statement

The data that support the findings of this study are available in the supplementary material of this article.

## Keywords

active matter, bismuth vanadate, photodeposition

Received: November 7, 2022

Revised: December 15, 2022

Published online:

- [1] J. L. Anderson, *Annu. Rev. Fluid Mech.* **1989**, *21*, 61.
- [2] R. Golestanian, T. Liverpool, A. Ajdari, *New J. Phys.* **2007**, *9*, 126.
- [3] L. Baraban, *Ph.D. thesis*, University of Konstanz, Germany, **2008**.
- [4] Y. Ibrahim, R. Golestanian, T. B. Liverpool, *J. Fluid Mech.* **2017**, *828*, 318.
- [5] R. Kapral, *J. Chem. Phys.* **2013**, *138*, 020901.
- [6] L. Feuerstein, C. G. Biermann, Z. Xiao, C. Holm, J. Simmchen, *J. Am. Chem. Soc.* **2021**, *143*, 17015.
- [7] W. Gao, A. Uygun, J. Wang, *J. Am. Chem. Soc.* **2012**, *134*, 897.
- [8] W. Gao, M. D'Agostino, V. Garcia-Gradilla, J. Orozco, J. Wang, *Small* **2013**, *9*, 467.
- [9] W. Gao, X. Feng, A. Pei, Y. Gu, J. Li, J. Wang, *Nanoscale* **2013**, *5*, 4696.
- [10] W. Duan, R. Liu, A. Sen, *J. Am. Chem. Soc.* **2013**, *135*, 1280.
- [11] P. Bayati, A. Najafi, *J. Chem. Phys.* **2016**, *144*, 134901.
- [12] X. Wang, L. Baraban, A. Nguyen, J. Ge, V. R. Misko, J. Tempere, F. Nori, P. Formanek, T. Huang, G. Cuniberti, J. Fassbender, D. Makarov, *Small* **2018**, *14*, 1803613.
- [13] C. Zhou, H. Zhang, J. Tang, W. Wang, *Langmuir* **2018**, *34*, 3289.
- [14] M. De Corato, X. Arqué, T. Patino, M. Arroyo, S. Sánchez, I. Pagonabarraga, *Phys. Rev. Lett.* **2020**, *124*, 108001.
- [15] A. Walsh, Y. Yan, M. N. Huda, M. M. Al-Jassim, S.-H. Wei, *Chem. Mater.* **2009**, *21*, 547.
- [16] S. Heckel, J. Simmchen, *Adv. Intell. Syst.* **2019**, *1*, 1900093.
- [17] S. Heckel, J. Grauer, M. Semmler, T. Gemming, H. Löwen, B. Liebchen, J. Simmchen, *Langmuir* **2020**, *36*, 12473.
- [18] M. Wittmann, S. Heckel, F. Wurl, Z. Xiao, T. Gemming, T. Strassner, J. Simmchen, *Chem. Commun.* **2022**, *58*, 4052.
- [19] R. Li, H. Han, F. Zhang, D. Wang, C. Li, *Energy Environ. Sci.* **2014**, *7*, 1369.
- [20] K. Villa, F. Novotny, J. Zelenka, M. P. Browne, T. Ruml, M. Pumera, *ACS nano* **2019**, *13*, 8135.
- [21] J. Simmchen, J. Katuri, W. E. Uspal, M. N. Popescu, M. Tasinkevych, S. Sánchez, *Nat. Commun.* **2016**, *7*, 10598.
- [22] S. Heckel, J. Hübner, A. Leutzgen, G. Jung, J. Simmchen, *Catalysts* **2021**, *11*, 599.
- [23] M. Náfrádi, L. Farkas, T. Alapi, K. Hernádi, K. Kovács, L. Wojnárovits, E. Takács, *Radiat. Phys. Chem.* **2020**, *170*, 108610.
- [24] D. K. Lee, K.-S. Choi, *Nat. Energy* **2018**, *3*, 53.
- [25] K. Wenderich, G. Mul, *Chem. Rev.* **2016**, *116*, 14587.
- [26] B. Xie, H. Zhang, P. Cai, R. Qiu, Y. Xiong, *Chemosphere* **2006**, *63*, 956.
- [27] S. Heckel, C. Bilsing, M. Wittmann, T. Gemming, L. Büttner, J. Czarne, J. Simmchen, *Adv. Sci.* **2022**, *9*, 2105009.
- [28] N. Tarantino, J.-Y. Tinevez, E. F. Crowell, B. Boisson, R. Henriques, M. Mhlanga, F. Agou, A. Israël, E. Laplantine, *J. Cell Biol.* **2014**, *204*, 231.